

# Shear behaviour of hybrid fibre-reinforced SCC T-beams

## Zhi-guo You

Associate Professor, College of Civil and Architectural Engineering, North China University of Science and Technology, Tangshan, P. R. China

## Xing-guo Wang

Professor, College of Civil and Architectural Engineering, North China University of Science and Technology, Tangshan, P. R. China

## Guo-huan Liu

Associate Professor, State Key Laboratory of Water Hydraulic Engineering Simulation and Safety, Tianjin University, Tianjin, P. R. China  
(corresponding author: liugh@tju.edu.cn)

## Hai-bin Chen

Professor, College of Civil and Architectural Engineering, North China University of Science and Technology, Tangshan, P. R. China

## Shi-xia Li

Senior engineer, Tianjin ZhongYi Architecture & Planning Design Co. Ltd, Tianjin, P. R. China

Three series of simply supported hybrid-fibre-reinforced self-compacting concrete T-beams subjected to four-point symmetrically placed vertical load were experimentally investigated. The influence of the following variables was studied: the fibre type, the fibre content, the stirrup ratio and the flange size. Failures were consistently shear or shear–flexure failures, except in five T-beam specimens where the failure was dominated by flexural cracks. The results showed that hybrid fibres can evidently enhance the ultimate shear load. The addition of hybrid fibres in adequate amounts can change the failure mode. The influence of different flange size on the ultimate shear load of the T-beams should be considered. Three methods were proposed – the ‘effective width’, ‘form factor’ and ‘shear funnel’ – for predicting the ultimate shear load of steel-fibre-reinforced self-compacting concrete T-beams, and another two methods were proposed – the ‘revised  $\sigma$ – $w$  design method’ and ‘revised  $\sigma$ – $\varepsilon$  design method’ – for predicting the ultimate shear load of hybrid fibre or steel-fibre-reinforced self-compacting concrete T-beams. The ultimate shear load recorded experimentally was compared with the value obtained from the proposed equation. The ‘revised  $\sigma$ – $w$  design method’ was more suitable for predicting the ultimate shear load of T-beams containing hybrid fibres and/or with stirrups, and the correlation was satisfactory.

## Notation

$A$	area of shaded part of cross-section	$f_{cu}$	cubic compressive strength
$a/d$	shear span–depth ratio	$f_{eq,2}$	equivalent flexural tensile strength according to $D_{f2}$
$b$	beam width	$f_{eq,3}$	equivalent flexural tensile strength according to $D_{f3}$
$b_{ef}$	‘effective width’ of a T-beam in shear	$f_L$	limit of proportionality
$b_f$	flange width	$f_{R,1}, f_{R,2},$	residual flexural tensile strengths corresponding to
$b_w$	web width, that is, rectangular beam width, $b$	$f_{R,3}, f_{R,4}$	midspan deflections of 0.46 mm, 1.31 mm, 2.15 mm, 3.00 mm, respectively
$b_2$	$Y$ -intercept of the second linear curve	$f_{y1}$	yield strength of longitudinal reinforcement
$c$	distance from extreme compression fibre to neutral axis	$f_{yst}$	yield strength of stirrup
$D_c$	energy absorption capacity of plain concrete	$h$	average of the difference in height between concrete inside and outside bars at four locations in the J-ring test
$D_{f2}$	energy absorption capacity, equal to the area under the load–deflection curve up to a deflection $\delta_2$ , $\delta_2 = \delta_L + 0.65$ mm, where $\delta_L$ is the deflection at the limit of proportionality	$h_f, t$	flange thickness
$D_{f3}$	energy absorption capacity, equal to the area under the load–deflection curve up to a deflection $\delta_3$ , $\delta_3 = \delta_L + 2.65$ mm	$I_b$	index of beam action
$d$	effective depth	$k_f$	factor for taking into account the contribution of the flanges in a $T$ -section according to Rilem TC 162-TDF $\sigma$ – $\varepsilon$ design method
$d_a$	maximum size of coarse aggregate	$k_1$	factor for taking into account the influence of the effective depth ‘ $d$ ’ according to Rilem TC 162-TDF $\sigma$ – $\varepsilon$ design method
$d_f$	equivalent diameter of fibre	$l_f$	fibre length
$d_1$	average final diameter in slump flow test	$l_f/d_f$	fibre aspect ratio
$d_2$	average final diameter in J-ring test	$s$	stirrup spacing
$F$ – $\Delta$	shear load–displacement curves	$T_{500}$	time taken for concrete to reach 500 mm spread circle in slump flow test
$F_u$	ultimate shear load		
$f'_c$	compressive strength of circular cylinder		

$u$	crack opening width
$V$	shear load
$V_{cd}$	ultimate shear load of member without shear reinforcement
$V_f$	contribution of fibres to shear load
$V_{fd}$	contribution of steel fibre shear reinforcement
$V_{Rd,3}$	ultimate shear load of a beam with shear reinforcement and containing steel fibres according to Rilem TC 162-TDF $\sigma$ - $\epsilon$ design method
$V_s$	contribution of stirrups to shear load
$V_{test}/V_{predicted}$	ratio of experimental ultimate shear load to predicted values
$V_{uc}$	contribution of concrete to shear load
$V_{uf}$	shear load of rectangular beams with steel fibres and stirrups
$V_{wd}$	contribution of shear reinforcement due to stirrups and/or inclined bars
$v_a$	shear stresses due to arch actions
$v_b$	shear stresses due to beam actions
$v_f$	contribution of fibres to shear strength
$v_s$	contribution of stirrups to shear strength
$v_u$	shear strength
$v_{uc}$	contribution of concrete to shear strength
$v_{uf}$	average shear strength of rectangular beams with steel fibres and stirrups
$z$	inner lever arm according to Rilem TC 162-TDF $\sigma$ - $\epsilon$ design method
$\alpha$	inclination between longitudinal reinforcement and shear crack
$\alpha_1$	slope of first linear curve
$\alpha_2$	slope of second linear curve
$\Delta_u$	ultimate displacement corresponding to $F_u$ at load point
$\theta$	the inclination between the neutral axis and the two angled lines
$\xi$	factor for taking into account size effect
$\rho_s$	longitudinal reinforcement ratio
$\rho_{st}$	stirrup ratio evaluated with reference to the spacing, $s$
$\bar{\sigma}_{p,d}$	the mean design residual stress at the crack width $w_m$
$\sigma_{w,d}$	the design stress-crack opening relationship
$\tau$	the average fibre matrix interfacial bond stress, $\tau = 4.15$ MPa

## Introduction

Cases with reinforced concrete T-section beams are very commonly encountered in practice. In international codes, such as the Chinese code GB 50010 (Ministry of Housing and Urban-Rural Construction of the People's Republic of China, 2010), ACI building code ACI 318-02 (ACI, 2002) and Eurocode 2 (BS EN 1992-1-1 (BSI, 2004)), the shear force in a T-beam is assumed to be carried only by its web. Previous studies have shown that the shear strength of a T-beam is, in many cases,

considerably higher than that of the rectangular beams of its web (Giaccio *et al.*, 2006; Tureyen *et al.*, 2006; Zararis *et al.*, 2006). A theory has been presented regarding the shear strength of reinforced concrete T-beams subjected to shear and flexure, and an effective width suitable for predicting the shear strength of T-beams was used (Zararis *et al.*, 2006). Three methods – the ‘form factor approach’, ‘shear-funnel method’ and ‘ignoring the flanges’ – were developed to extend a shear design equation that was previously derived for rectangular sections to T-sections (Tureyen *et al.*, 2006). The proposed shear methods were used to calculate shear strengths of 154 T-beams and 370 rectangular beams from 32 different investigations, and the calculated values were shown to correlate well with the experimental results.

The shear bearing capacity of rectangular beams under bending and shear can be improved by steel fibres. Previous studies have already proved the physical and mechanical advantages of steel fibres in terms of the concrete shear performance (Cucchiara *et al.*, 2004; Ding *et al.*, 2011, 2012; Han *et al.*, 2015; Kwak *et al.*, 2002; Zhang *et al.*, 2016). The incorporation of hybrid fibres in concrete improves the tensile strength moderately and the toughness considerably (Abadel *et al.*, 2016). Hybrid fibres can replace the confinement to some extent, whereby the congestion of reinforcement can be avoided (Ganesan *et al.*, 2016). Ding *et al.* (2010) evaluated the influence of different fibre types, for example, steel macro-fibre and hybrid fibre (macro steel fibre + macro plastic fibre) on the shear toughness and shear strength of reinforced concrete rectangular beams. The results indicated that hybrid fibres can evidently enhance the ultimate shear bearing capacity. However, no research on the shear behaviour of hybrid-fibre-reinforced T-beams has been reported.

Fibre-reinforced self-compacting concrete (FRSCC) combines the advantages of traditional fibre-reinforced concrete (FRC) and self-compacting concrete (SCC). The post-cracking behaviour mainly determines the fibre dosage of FRC; however, the workability of fresh SCC strongly restricts the fibre dosage of FRSCC (Ding *et al.*, 2008). Greenough and Nehdi (2008) concluded that the shear behaviour of FRSCC beams without stirrups was better than that of common FRC beams without stirrups because of the more homogeneous dispersion of fibres in FRSCC. The construction costs and period may be markedly reduced by using FRSCC. Thin or irregularly shaped sections, where it may be very difficult to place stirrups, can also be easily placed by FRSCC.

This paper analyses the influence of hybrid fibres and/or stirrups on the structural performance of SCC T-beams subjected mainly to shear forces, the influence of hybrid fibres or steel fibres on the failure mode and the ultimate shear load, and the influence of different flange size on the ultimate shear load of T-beams. Three methods – the ‘effective width’, ‘form factor’ and ‘shear-funnel’ methods – for predicting the

ultimate shear load of steel-fibre-reinforced SCC T-beams, and another two methods – the ‘revised  $\sigma-w$  design method’ and the ‘revised  $\sigma-\varepsilon$  design method’ for predicting the ultimate shear load of hybrid-fibre- or steel-fibre-reinforced SCC T-beams are proposed. The validity of the proposed equations is verified.

## Experimental programme

### Beams and set-up description

Three series of hybrid-fibre-reinforced SCC T-beams (B, C and D) were prepared. A half T-beam (out of the experimental zones) was stiffened, so that the other half T-beam (testing areas) would fail in shear collapse first. The systemic measurement of displacement and strain was to be obtained in the testing areas of the beam. The stirrup ratio of every T-beam stiffened out of the experimental zones was larger than that of the testing areas.

All of the T-beams were 1750 mm long. The thicknesses of the flange and flange widths of the three series of T-beams were different. The span of all the T-beams was 1500 mm. Two stirrup ratios and four fibre contents were selected. The first stirrup ratio was 0.35%, referring to the Chinese code, GB 50010 (Ministry of Housing and Urban-Rural Construction of the People’s Republic of China, 2010), for the minimum stirrup ratio. The second stirrup ratio was 0.53%, which is larger than the minimum stirrup ratio. Four fibre contents of 20 kg/m<sup>3</sup> (steel fibre), 20 + 6 kg/m<sup>3</sup> (steel fibre + plastic fibre),

40 kg/m<sup>3</sup> (steel fibre) and 40 + 4 kg/m<sup>3</sup> (steel fibre + plastic fibre) separately were determined by the workability of fresh SCC. The shear span-to-depth ratio was 3.2 and the longitudinal reinforcement ratio was 3.38% in all T-beams. The diameter of the longitudinal reinforcement was 25 mm (two longitudinal reinforcements). The parameters of the three series of T-beams are provided in Table 1.

All T-beam specimens were tested as simply supported beams under a two-point loading condition. Electrical strain gauges were installed to the longitudinal reinforcement under the loading point, at mid-span and under a point 212.5 mm distant from the support. The strain gauges were also installed to every stirrup in the testing span. In order to measuring T-beam deflection at mid-span, loading point and support, five linear variable differential transformers (LVDTs) were used. The longitudinal gauges were applied at locations across the width of the flange and throughout the depth. Crack gauges were provided in the shear span for measuring crack width. The experimental set-up has a capacity of 10 000 kN. A load transducer with 500 kN was used for measuring the load. The mid-span displacement of the T-beam increased at a constant rate of 0.2 ( $\pm 0.02$  mm/min) until a specified load. The specified load was kept constant until the measurements by LVDT, strain and crack gauges did not change. The values from the load transducer, LVDTs and strain gauges were continuously collected. Figure 1 shows a schematic diagram of the loading and some arrangements of the T-beams.

Table 1. Parameters of B, C and D series of T-beams

Beam no.	Web width: mm	Web height: mm	Flange width: mm	Flange thickness: mm	Testing areas			Steel fibre content: kg/m <sup>3</sup>	Plastic fibre content: kg/m <sup>3</sup>
					Stirrup diameter: mm	Stirrup space: mm	Stirrup ratio		
B1	125	190	240	60	0	$\infty$	0	0	0
B2	125	190	240	60	0	$\infty$	0	20	6
B3	125	190	240	60	0	$\infty$	0	40	0
B4	125	190	240	60	6.5	150	0.35%	0	0
B5	125	190	240	60	6.5	150	0.35%	20	6
B6	125	190	240	60	6.5	150	0.35%	40	0
C1	125	160	240	90	0	$\infty$	0	0	0
C2	125	160	240	90	0	$\infty$	0	20	0
C3	125	160	240	90	0	$\infty$	0	20	6
C4	125	160	240	90	0	$\infty$	0	40	0
C5	125	160	240	90	0	$\infty$	0	40	4
C6	125	160	240	90	6.5	150	0.35%	0	0
C7	125	160	240	90	6.5	150	0.35%	20	0
C8	125	160	240	90	6.5	150	0.35%	20	6
C9	125	160	240	90	6.5	150	0.35%	40	0
C10	125	160	240	90	6.5	150	0.35%	40	4
C11	125	160	240	90	6.5	100	0.53%	0	0
D1	125	160	360	90	0	$\infty$	0	0	0
D2	125	160	360	90	0	$\infty$	0	20	6
D3	125	160	360	90	0	$\infty$	0	40	0
D4	125	160	360	90	6.5	150	0.35%	0	0
D5	125	160	360	90	6.5	150	0.35%	20	6
D6	125	160	360	90	6.5	150	0.35%	40	0

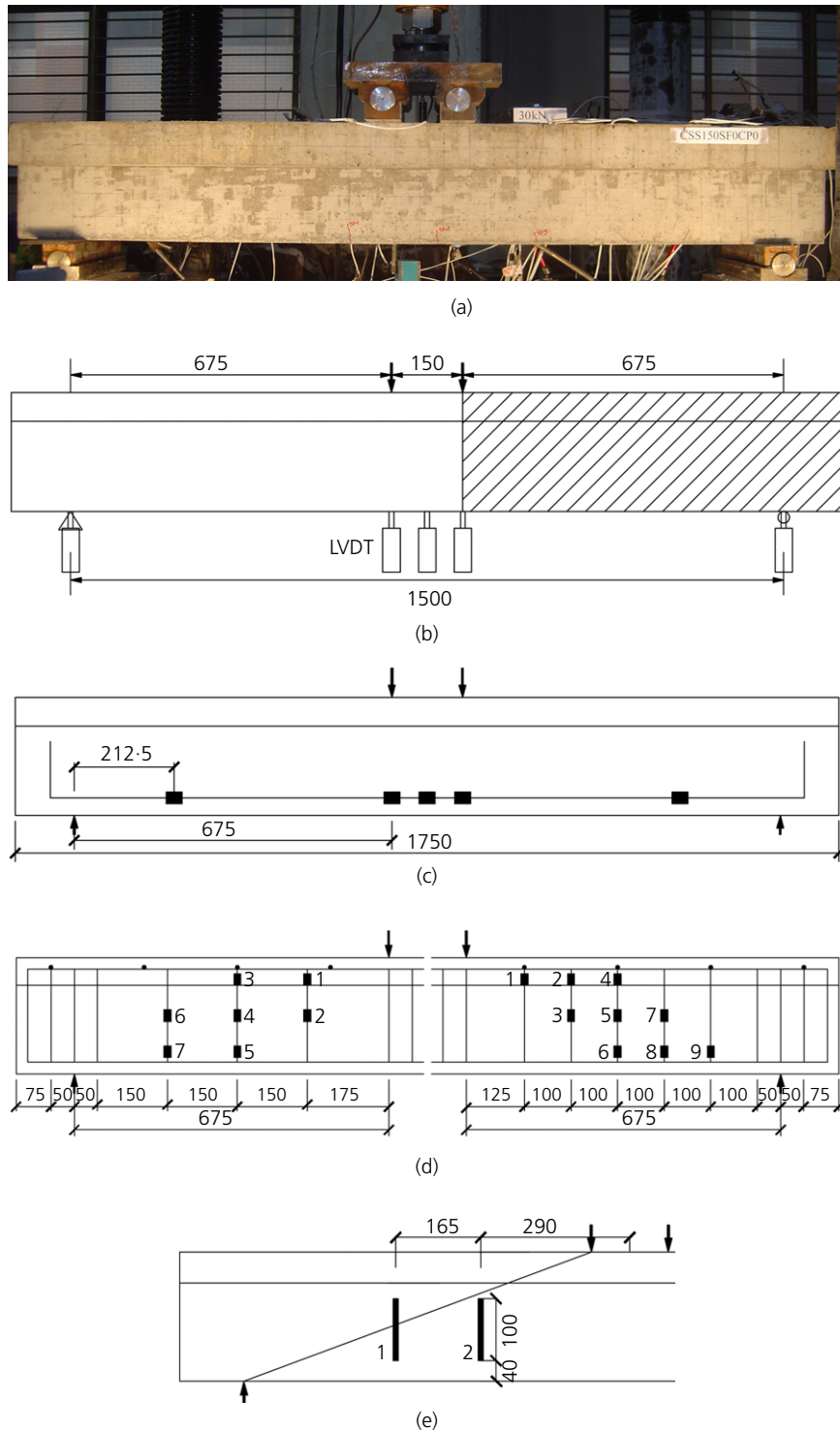


**Figure 1.** Schematic diagram of loading and some arrangements of T-beam: (a) schematic diagram of loading; (b) LVDT layout; (c) longitudinal reinforcement strain gauges; (d) stirrup strain gauges; (e) crack gauges

### Materials

The matrix materials were: cement, PO 42.5 Portland cement; fly ash, type I; fine aggregate, natural river sand; coarse aggregate, crushed stone with particle size 5–10 mm; superplasticiser,

polycarboxylate superplasticiser. The details of the SCC mixture proportions are presented in Table 2. A large amount of the workability test was carried out based on Efnarc (2002) and *SCC 028* guidelines (EPG, 2005). The mixing time was

Table 2. Mix proportions

Cement: kg/m <sup>3</sup>	Fly ash: kg/m <sup>3</sup>	Water: kg/m <sup>3</sup>	Sand: kg/m <sup>3</sup>	Gravel: kg/m <sup>3</sup>	Super-plasticiser: %	w/b: %
388.5	166.5	210	769.4	710.2	0.9	0.38

Table 3. Fibre parameters

Fibre type	Fibre geometry	Fibre length: mm	Diameter: mm	Fibre aspect ratio	Modulus of elasticity: GPa	Density: g/cm <sup>3</sup>	Fibre number per kg
Steel fibre	Hooked-end fibre	35	0.55	64	200	7.85	14 500
Plastic fibre (polymer fibre)	Straight fibre	30	0.66	45	35.7	1.3	75 540

also rigorously controlled according to Efnarc (2002) and SCC 028 guidelines (EPG, 2005). A trained and experienced technician can judge the quality of fresh fibre SCC. Steel fibres (SF) and plastic fibres (PF) were used for the SCC. Table 3 lists the fibre parameters in detail. In this paper, the hybrid SF and PF used in Table 3 are hybrids based on the fibre constitutive response. One type of fibre is stronger and stiffer and provides reasonable first crack strength and ultimate strength, whereas the second type of fibre is relatively flexible and leads to improved toughness and strain capacity in the post-crack zone.

The longitudinal reinforcement and stirrup have an average yield strength of 465.6 MPa and 354.4 MPa, respectively, and an average tensile strength of 653.9 MPa and 526.9 MPa, respectively.

### Test methods of workability

The workability of fresh SCC can be studied according to Ding *et al.* (2005), Efnarc (2002) and the SCC 028 guidelines (EPG, 2005). The test methods operated in this test include the slump flow test (for assessing the workability and filling ability) and the J-ring test (for assessing passing ability and flowability, as well segregation resistance). For example, tests of workability of SCC with 20 kg/m<sup>3</sup> SF + 6 kg/m<sup>3</sup> PF and 40 kg/m<sup>3</sup> SF + 6 kg/m<sup>3</sup> PF can be seen in Figure 2. They are sufficient to monitor production quality (Efnarc, 2002; SCC 028 (EPG, 2005)).

From Figure 2, it can be seen that the workability (flowability, segregation resistance, passing ability and filling ability) of the fibre-reinforced fresh mixture with 20 kg/m<sup>3</sup> SF + 6 kg/m<sup>3</sup> PF fulfils the requirement of SCC (Efnarc, 2002; SCC 028 (EPG, 2005)). However, the workability of the fibre-reinforced fresh mixture with 40 kg/m<sup>3</sup> SF + 6 kg/m<sup>3</sup> PF cannot fulfil the requirement.

## Results

### Test results of workability and cubic compressive strength

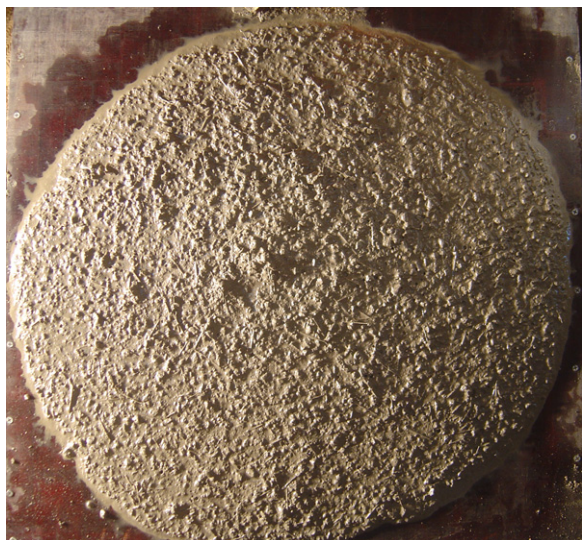
Table 4 gives the experimental results for workability of the hybrid fibre-reinforced SCC. These results indicate that all

parameters correspond well to the requirements, except for the mixture with 40 kg/m<sup>3</sup> SF + 6 kg/m<sup>3</sup> PF (Efnarc, 2002; SCC 028 (EPG, 2005)). When the hybrid fibre content was 40 + 4 kg/m<sup>3</sup>, the height difference between inside and outside steel rebars in the J-ring test was equal to 15 mm, which just fulfilled the requirements ( $h \leq 15$  mm) (Efnarc, 2002; SCC 028 (EPG, 2005)). The average of the difference in height between the concrete just inside the bars and that outside the bars at four locations in the J-ring test was 20 mm beyond the limit of 15 mm (see in Table 4 and Figure 2(c)). This means that the hybrid fibre content of 40 + 4 kg/m<sup>3</sup> could achieve the upper limit of the workability of FRSCC. The cubic specimen size was 150 mm × 150 mm × 150 mm. Table 4 also gives the values of cubic compressive strength,  $f_{cu}$ , at the age of 120 d (at the time of testing).

### Shear load–displacement curves

#### Shear load–displacement curves of T-beams without stirrups and fibres

Figures 3 and 4 show shear load–displacement curves (i.e.  $F-\Delta$  curves) and the crack patterns of B1, C1 and D1 T-beams, respectively. As a displacement-controlled test was performed, any damage induced in the structure generated a drop in the applied force and a decrease in the slope of the shear load–displacement curve. It can be seen that flexural cracks were formed at mid-span and shear span first. Then, an inclined crack formed along some flexural cracks with the increment of displacement. When the critical crack formed, an important drop in the applied load occurred suddenly, but with the increment of displacement, the resisted load increased and the stiffness decreased with the formation of successive cracks. The first shear load peak occurred. The diagonal critical shear cracks ran from the mid-height of the web to the loading point at the top and to the support at the bottom with the increment of displacement. The principal and critical shear crack had a shallow angle through the flange, crossed the interface between the flange and the web, and reached the compression zone of the beam. These beams were able to resist higher shear load after the formation of new diagonal cracks, as the arch action was developed, and finally collapsed by a diagonal and sudden shear failure. The second shear load peak occurred. In the B1,



(a)



(b)



(c)

**Figure 2.** Tests of workability of SCC with 20 kg/m<sup>3</sup> SF + 6 kg/m<sup>3</sup> PF and 40 kg/m<sup>3</sup> SF + 6 kg/m<sup>3</sup> PF: (a) slump flow test with SF 20 kg/m<sup>3</sup> and PF 6 kg/m<sup>3</sup>; (b) J-ring test with SF 20 kg/m<sup>3</sup> and PF 6 kg/m<sup>3</sup>; (c) J-ring of SCC with SF 40 kg/m<sup>3</sup> and PF 6 kg/m<sup>3</sup>

C1 and D1 T-beams, longitudinal reinforcement did not reach yielding at the second shear load peak. The B1, C1 and D1 T-beams failed in shear collapse.

#### Shear load–displacement curves of B, C and D series of T-beams

Figures 5, 6 and 7 show the comparison of shear load–displacement curves of the B, C and D series of T-beams without stirrups, respectively. Table 5 lists the ultimate shear load, ultimate displacement and failure mode of B, C and D series of T-beams. The following points can be seen from Figures 5–7 and Table 5.

- Compared to beams B1, C1 and D1, the load-carrying capacity of hybrid fibre-reinforced RC beams (beams B2, C3, C5 and D2) performed much better over the entire displacement range, correspondingly. The displacement at the load point of the hybrid fibre-reinforced RC beams decreased under the same load before the peak load of the beam (except for beam C5). The stiffness of the hybrid fibre-reinforced RC beams increased appreciably because of fibres delaying cracks and limiting development of cracks. The ultimate shear load  $F_u$  and ultimate displacement  $\Delta_u$  corresponding to  $F_u$  at the load point of the hybrid fibre-reinforced RC beams increased clearly (see Table 5). Based on the above discussion, this means that the addition of hybrid fibres can enhance the toughness greatly.
- Compared to beam C2 (with 20 kg/m<sup>3</sup> mono-SF, without stirrups), although beam C3 has more fibres (hybrid 20 kg/m<sup>3</sup> SF and 6 kg/m<sup>3</sup> PF, without stirrups), the displacement at the load point of the beam C3 in the pre-peak region increased under the same load. The stiffness of the beam C3 decreased appreciably. More experiments should be conducted to evaluate this phenomenon. The ultimate shear load  $F_u$  of the beam C3 increased by about 9%, and the ultimate displacement  $\Delta_u$  corresponding to  $F_u$  at the load point increased by 38% (see Table 5). The post-peak load-carrying capacities of the beam C3 are better than that of beam C2. The similar character of beams C4 and C5 can be seen from Figure 6.
- Compared to the beam B3 (with 40 kg/m<sup>3</sup> mono-SF, without stirrups), the displacement at the load point of the beam B2 (hybrid 20 kg/m<sup>3</sup> SF and 6 kg/m<sup>3</sup> PF, without stirrups) under the same load decreased before about 85 kN, and increased after about 85 kN until the shear load peak of B3. The similar character between beams D2 and D3 can be seen from Figure 7. However, compared to the beam C4 (with 40 kg/m<sup>3</sup> mono-SF, without stirrups), the displacement at the load point of the beam C3 (hybrid 20 kg/m<sup>3</sup> SF and 6 kg/m<sup>3</sup> PF, without stirrups) under the same load increased until the shear load peak of C4. The ultimate shear load  $F_u$  and

Table 4. Test results of workability and cubic compressive strength

Fibre type: kg/m <sup>3</sup>	Slump flow test		J-ring test		Cubic compressive strength $f_{cu}$ : MPa
	$d_1$ : mm	$T_{500}$ : s	$d_2$ : mm	$h$ : mm	
SF0PF0	780	3.0	780	1	47.71
SF20PF0	770	3.3	740	2	46.62
SF20PF6	740	4.1	700	10	49.07
SF40PF0	760	3.8	730	8	33.73
SF40PF4	730	4.5	700	15	36.03
SF40PF6	700	5.0	660	20	—

Note: The fibre type of SF20PF6 denotes the FRSCC with 20 kg/m<sup>3</sup> steel fibre (SF) and 6 kg/m<sup>3</sup> plastic fibre (PF). The first number indicates SF content; the second number indicates PF content

the ultimate displacement  $\Delta_u$  corresponding to  $F_u$  at the load point of the beams B2, D2 and C3 all increased compared to the beams B3, D3 and C4, respectively. The post-peak load of the beams B2, D2 and C3 dropped significantly compared to the beams B3, D3 and C4, respectively.

- (d) The shear behaviour of beams C2 and C3 is better than that of beams C4 and C5, respectively. However, the fibre contents of beams C4 and C5 are higher than those of beams C2 and C3, respectively. This phenomenon is not reasonable and is inconsistent with previous studies (Ding *et al.*, 2010). The reason may be poor curing of beams C4 and C5. Therefore, the beams C4 and C5 were not considered for further analysis.
- (e) The B, C and D series of T-beams without stirrups all failed in shear collapse.

To assess the effectiveness of stirrups replaced by hybrid fibres or steel fibres, the shear behaviour of the beam with just fibres (without stirrups) that behaved with the best shear performance was compared to that of the beam with just the lowest quantity of stirrups. The shear load–displacement curves of beams B2, C3 and D2 with just fibres (hybrid fibres 20 + 6 kg/m<sup>3</sup>) were compared to those of beams B4, C6 and D4 (stirrup ratio of 0.35%), respectively. Figures 8, 9 and 10 show the compared curves. The stirrup ratio of 0.35% (dia. 6.5@150) corresponds to the steel amount of 42 kg/m<sup>3</sup>.

The following points can be seen from Figures 8–10.

- (a) The stiffness of the beam B2 with just hybrid fibres before the shear load 95 kN is better than that of the beam B4 with just stirrups. However, after the shear load of 95 kN, the reverse phenomenon is observed. A similar trend can be found when comparing beams D2 and D4 (the intersected shear load is about 89 kN) and beams C3 and C6 (the intersected shear load is about 66 kN). The reason is that the three-dimensional distributed hybrid fibres act as effective shear reinforcement, and the fibres can be more effective in arresting crack propagation and

maintaining the integrity of the surrounding concrete at the early stage of loading. When the deformability is increased, much energy is absorbed in debonding and pulling hybrid fibres out of the concrete matrix. When the crack width is so large that the hybrid fibres are pulled out completely or pulled off, the hybrid fibres across the crack become fewer and fewer. However, this phenomenon would not appear in the beam with the stirrups as continuum shear reinforcement, and the stirrups did not fracture. Therefore, with the increase in load, the rate of stiffness reduction of the beam with just hybrid fibres exceeds that of the beam with just stirrups. The stiffness of the beam B4 with just stirrups is larger than that of the beam B2 with just hybrid fibres after the shear load 95 kN.

- (b) The ultimate shear load and the post-peak load-carrying capacities of the beams B4, C6 and D4 with just stirrups are all better than those of beams B2, C3 and D2 with just fibres.

This means that the load-carrying capacities between the beams B4, C6, D4 and the beams B2, C3, D2, respectively, are not equivalent. Also, the shear reinforcements (dia. 6.5@150, steel amount 42 kg/m<sup>3</sup>) in the current experiment cannot be totally replaced by only 20 + 6 kg/m<sup>3</sup> hybrid fibres. The addition of 20 + 6 kg/m<sup>3</sup> hybrid fibres cannot totally replace 42 kg/m<sup>3</sup> of stirrups.

The comparisons of the shear load–displacement curves of the B, C and D series of T-beams with stirrups (stirrup ratio,  $\rho_{st}$  = 0.35%, 0.53%) are shown in Figures 11, 12 and 13, respectively. The stirrup ratio of 0.53% (dia. 6.5@100) corresponds to the steel amount of 63 kg/m<sup>3</sup>. An assessment of the effectiveness the partial replacement of stirrups by hybrid fibres or steel fibres can be made. The composite effect of hybrid fibres and stirrups on the shear behaviour of beams can be evaluated.

Figure 14 shows the crack pattern and failure mode of the B, C and D series of T-beams with stirrups. The following observations can be made from Figures 11–14 and Table 5.

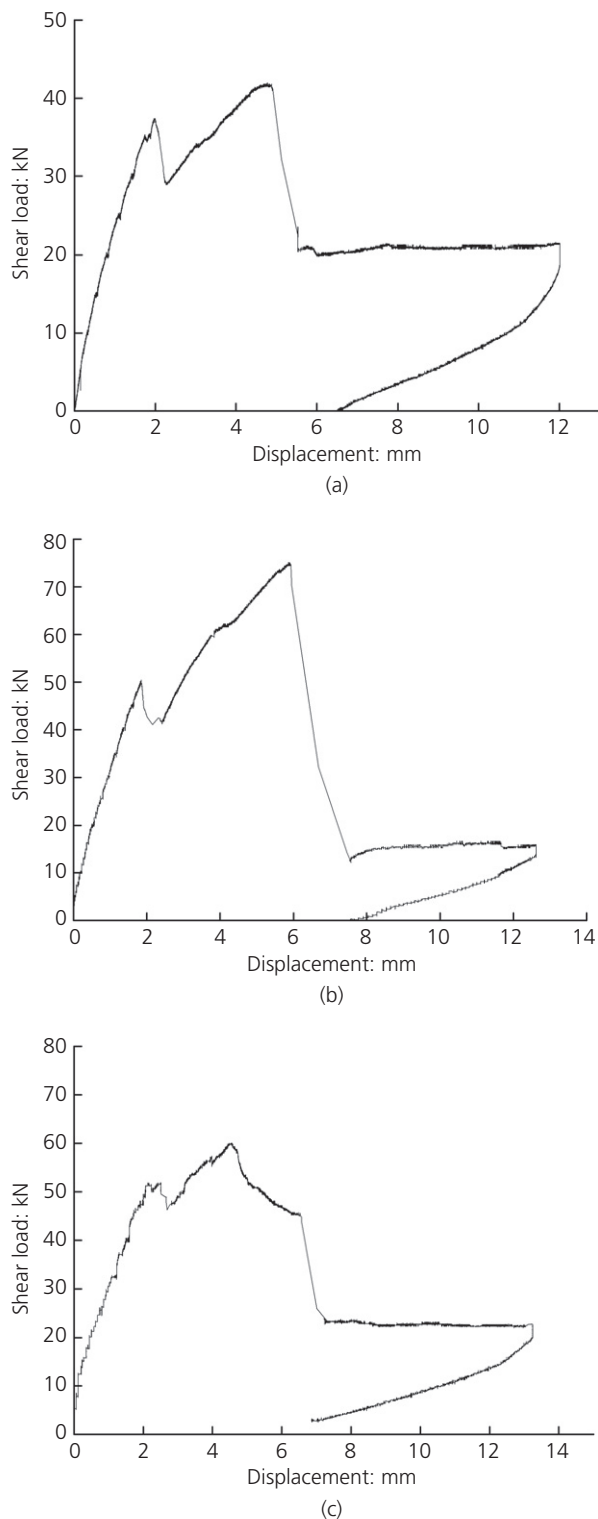


Figure 3. Shear load–displacement curves of T-beams without stirrups and fibres: (a) B1 T-beam; (b) C1 T-beam; (c) D1 T-beam

(a) The beam B4 with just stirrups (dia. 6.5@150) failed in shear collapse (see Figure 11). The addition of hybrid fibres 20 + 6 kg/m<sup>3</sup> to the beam B4 can transform the

failure mode into a more ductile one. The beam B6 failed in flexure collapse. This means that 20 + 6 kg/m<sup>3</sup> hybrid fibres can partially replace stirrups. The beam B5 with mixed steel fibres 40 kg/m<sup>3</sup> failed in flexure–shear collapse (see Figure 11). That is, the mid-span longitudinal reinforcement of beam B5 yielded. Also, the concrete strain on the edge of the compressive zone of beam B5 reached ultimate compressive strain. However, the mid-span longitudinal reinforcement stress did not reach the ultimate stress. The beam B5 finally failed in shear collapse. The maximum crack width was located in the shear span when the beam B5 failed.

- (b) The beam D4 with just stirrups (dia. 6.5@150) failed in flexure–shear collapse. The addition of hybrid fibres 20 + 6 kg/m<sup>3</sup> or steel fibres 40 kg/m<sup>3</sup> to the beam D4 can transform the failure mode into a more ductile one. The beams D5 and D6 failed in flexure collapse (see Figure 13). This means that hybrid fibres 20 + 6 kg/m<sup>3</sup> or steel fibres 40 kg/m<sup>3</sup> can partially replace stirrups.
- (c) A similar character can be seen during testing of beams C6–C11. However, the beam C8 with mixed hybrid fibres 20 + 6 kg/m<sup>3</sup> failed in flexure–shear collapse and the beam C9 with mixed steel fibres 40 kg/m<sup>3</sup> failed in flexure collapse. This phenomenon is different from beams B5 and B6, which contained the same mix of fibres. Possibly the improvement in the shear behaviour of the beams by the two types of fibres (20 + 6, 40 kg/m<sup>3</sup>) is similar.
- (d) Compared to the beam C11 with just a stirrup ratio of 0.53% (steel amount of 63 kg/m<sup>3</sup>) which failed in flexure–shear collapse, although the beams C9 and C10 (stirrup ratio of 0.35%, steel amount 42 kg/m<sup>3</sup>) had a smaller stirrup ratio, the addition of steel fibres 40 kg/m<sup>3</sup> or hybrid fibres 40 + 4 kg/m<sup>3</sup> to the beams C9 and C10 was able to transform the failure mode. The beams C9 and C10 failed in flexure collapse. This means that steel fibres 40 kg/m<sup>3</sup> or hybrid fibres 40 + 4 kg/m<sup>3</sup> can partially replace a stirrup amount of 21 kg/m<sup>3</sup> and enlarge the stirrup spacing from 100 mm to 150 mm under conditions where the shear span-to-depth ratio is 3.2.

This means that the combination of hybrid fibres and stirrups demonstrates a positive composite effect on shear behaviour. The addition of 20 + 6 kg/m<sup>3</sup> hybrid fibres, 40 + 4 kg/m<sup>3</sup> hybrid fibres and 40 kg/m<sup>3</sup> steel fibres may partially replace the stirrup amount of 21 kg/m<sup>3</sup>.

### The ultimate shear load of B, C and D series of T-beams and proposed predictive equation

#### The ultimate shear load

The influence of fibre contents on ultimate shear load of B, C and D series of T-beams are shown in Figure 15. The following observations can be made from Figure 15 and Table 5.

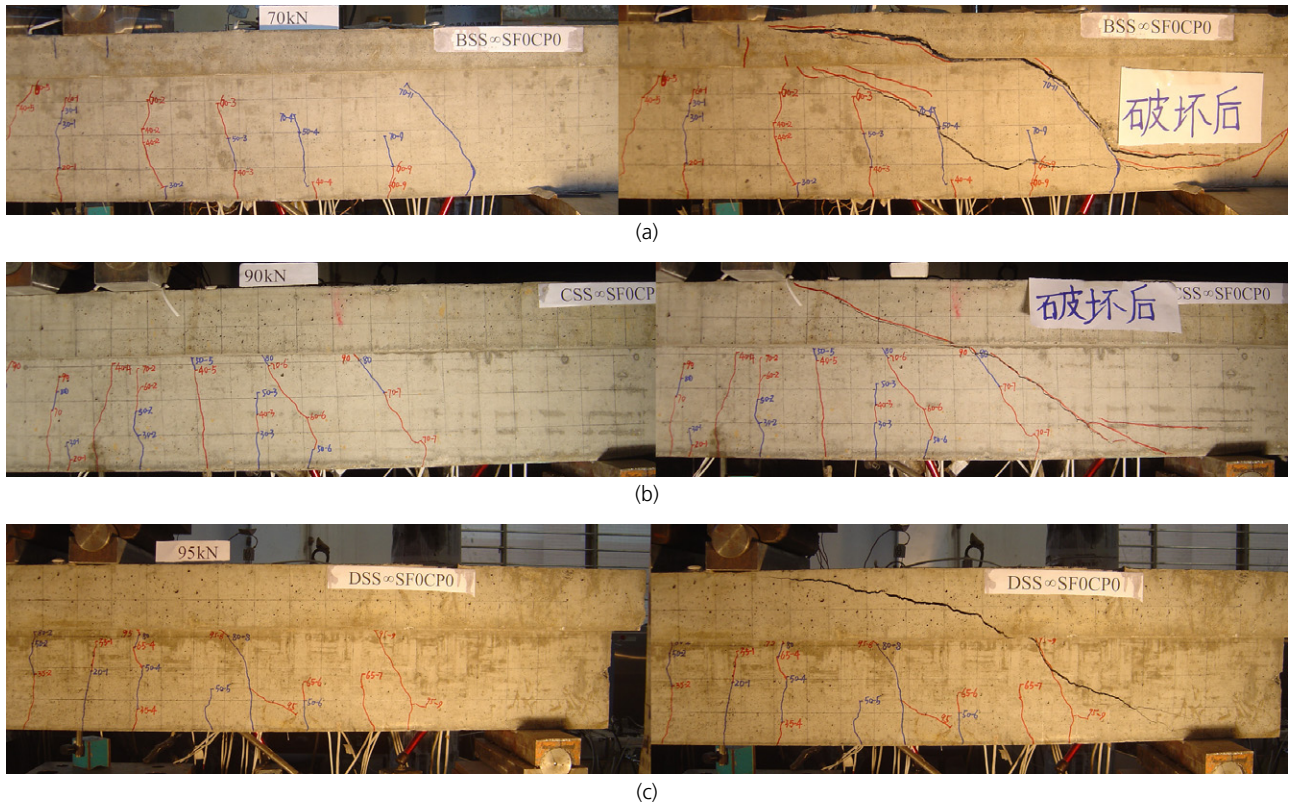


Figure 4. Crack pattern and failure mode of T-beams without stirrups and fibres: (a) B1 T-beam; (b) C1 T-beam; (c) D1 T-beam

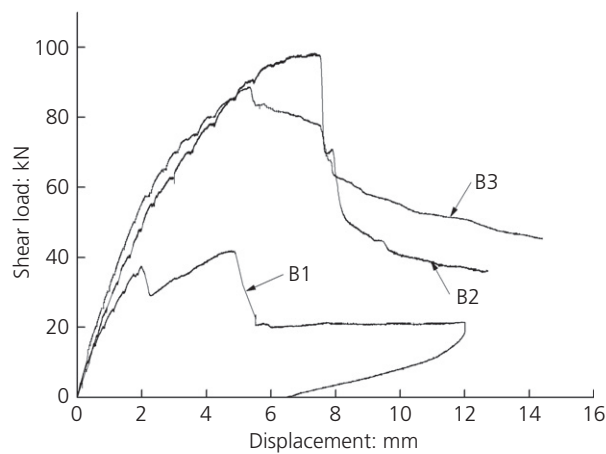


Figure 5. Shear load–displacement curves of B series of beams without stirrups

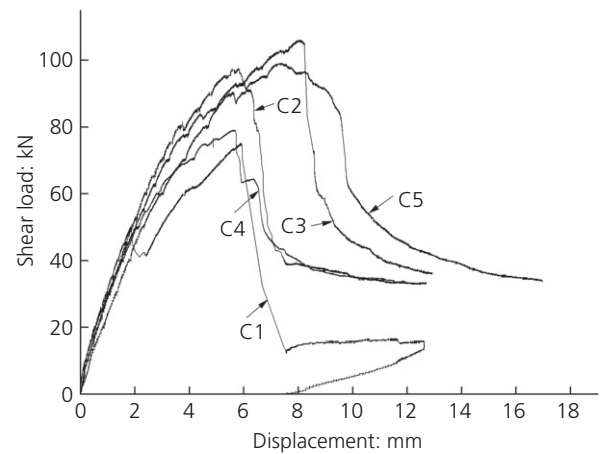


Figure 6. Shear load–displacement curves of C series of beams without stirrups

- (a) When fibre contents remain constant, the ultimate shear load increased with the increase of stirrup ratio.
- (b) For B, C and D series of T-beams without stirrups, a fibre content of  $20 + 6 \text{ kg/m}^3$  or  $40 \text{ kg/m}^3$  can enhance the ultimate shear load compared to the T-beam without fibres. The ultimate shear loads of T-beams with the

- addition of hybrid fibres  $20 + 6 \text{ kg/m}^3$  are better than those of T-beams with steel fibres  $40 \text{ kg/m}^3$ .
- (c) For B, C and D series of T-beams with stirrup ratio of 0.35%, a fibre content of  $20 + 6 \text{ kg/m}^3$  or  $40 \text{ kg/m}^3$  can also enhance the ultimate shear load compared to the T-beam without fibres. However, the comparison between

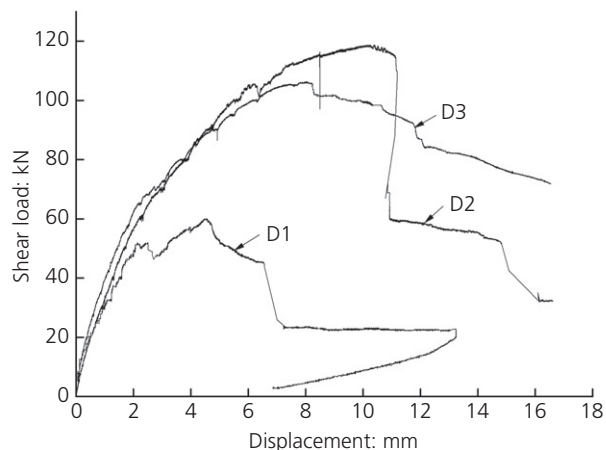


Figure 7. Shear load–displacement curves of D series of beams without stirrups

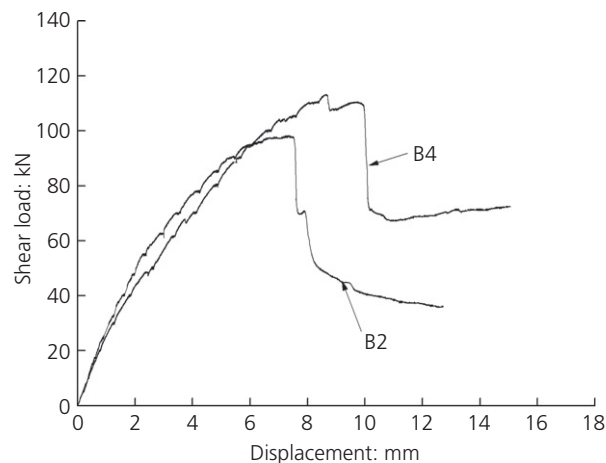


Figure 8. Shear load–displacement curves compared between B2 and B4

ultimate shear loads of T-beams with the addition of hybrid fibres  $20 + 6 \text{ kg/m}^3$  and steel fibres  $40 \text{ kg/m}^3$  is different for the B, C and D series of T-beams without stirrups. The ultimate shear loads of B5 T-beams (hybrid fibres  $20 + 6 \text{ kg/m}^3$ ) are better than those of B6 T-beams (steel fibres  $40 \text{ kg/m}^3$ ). The ultimate shear loads of C8 T-beams (hybrid fibres  $20 + 6 \text{ kg/m}^3$ ) are lower than those of C9 T-beams (steel fibres  $40 \text{ kg/m}^3$ ). The D5 and D6 T-beams failed in flexural collapse, and the ultimate shear loads of the two beams cannot be compared with each other. It is possible that the composite effect of hybrid

fibres  $20 + 6 \text{ kg/m}^3$  and steel fibres  $40 \text{ kg/m}^3$  with stirrups on the ultimate shear load is similar.

- (d) For the C series of T-beams, the T-beams with hybrid fibres  $40 + 4 \text{ kg/m}^3$  and steel fibres  $20 \text{ kg/m}^3$  are made and tested alongside the T-beams with hybrid fibres  $20 + 6 \text{ kg/m}^3$  and steel fibres  $40 \text{ kg/m}^3$ . The ultimate shear loads of T-beams with the addition of hybrid fibres  $20 + 6 \text{ kg/m}^3$  are better than those of T-beams with steel fibres  $20 \text{ kg/m}^3$ . The ultimate shear loads of T-beams with the addition of hybrid fibres  $40 + 4 \text{ kg/m}^3$  are better than those of T-beams with steel fibres  $40 \text{ kg/m}^3$ .

Table 5. Ultimate shear load, ultimate displacement and failure mode of B, C and D series of T-beams

Beam no.	Ultimate shear load: kN	Shear strength: MPa	Ultimate displacement at shear load point: mm	Failure mode
B1	41.95	1.58	1.97	Shear
B2	98.44	3.71	7.36	Shear
B3	88.75	3.34	5.29	Shear
B4	113.23	4.26	8.61	Shear
B5	>135.43	—	26.44	Flexure
B6	128.11	4.82	11.36	Flexure–shear
C1	75.12	2.83	1.94	Shear
C2	97.63	3.68	5.80	Shear
C3	106.10	3.99	8.03	Shear
C4	79.15	2.98	5.58	Shear
C5	99.26	3.74	7.41	Shear
C6	127.50	4.8	12.62	Flexure–shear
C7	130.29	4.9	8.98	Flexure–shear
C8	135.99	5.12	10.79	Flexure–shear
C9	>139.54	—	50.78	Flexure
C10	>151.68	—	38.33	Flexure
C11	135.80	5.11	13.26	Flexure–shear
D1	60.05	2.26	2.26	Shear
D2	119.58	4.5	10.25	Shear
D3	106.75	4.02	8.03	Shear
D4	128.05	4.82	9.88	Flexure–shear
D5	>145.53	—	35.21	Flexure
D6	>146.38	—	36.79	Flexure

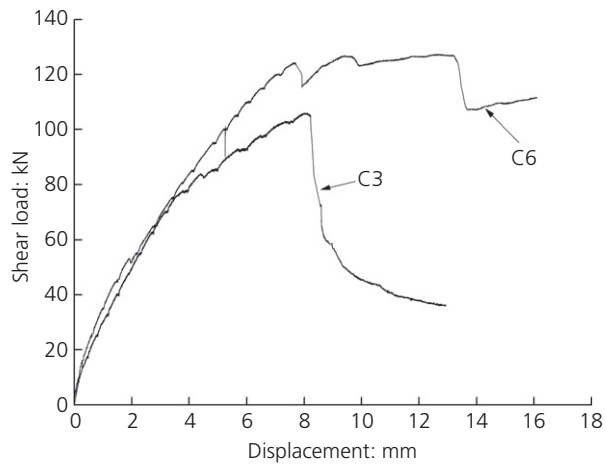


Figure 9. Shear load–displacement curves compared between C3 and C6

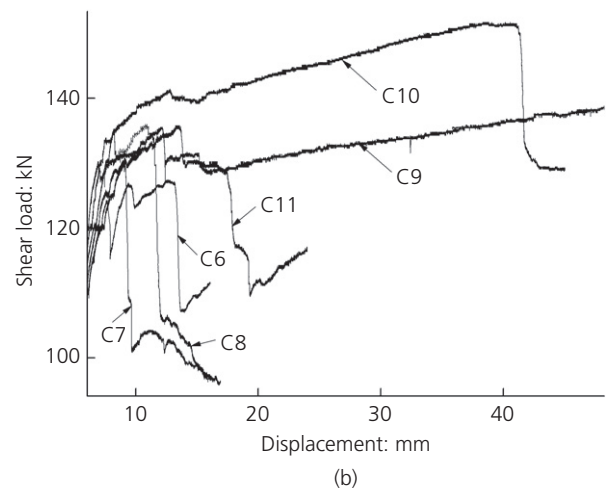
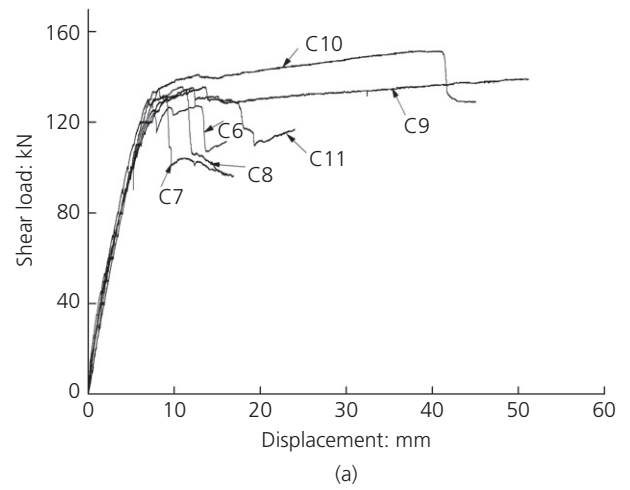


Figure 12. Shear load–displacement curves of C series of beams with stirrup ratios of 0.35%, 0.53%: (a) overall drawing; (b) partial enlarged detail

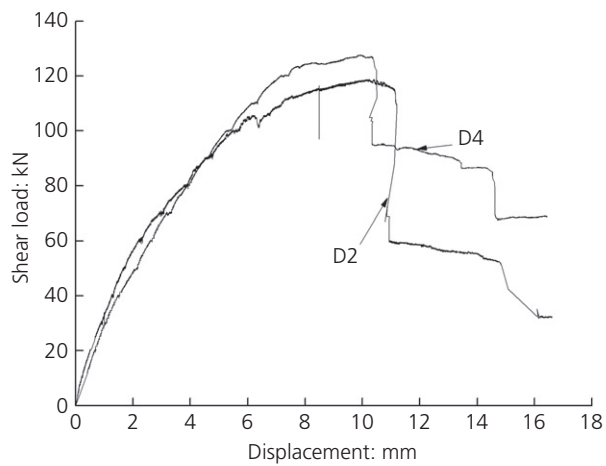


Figure 10. Shear load–displacement curves compared between D2 and D4

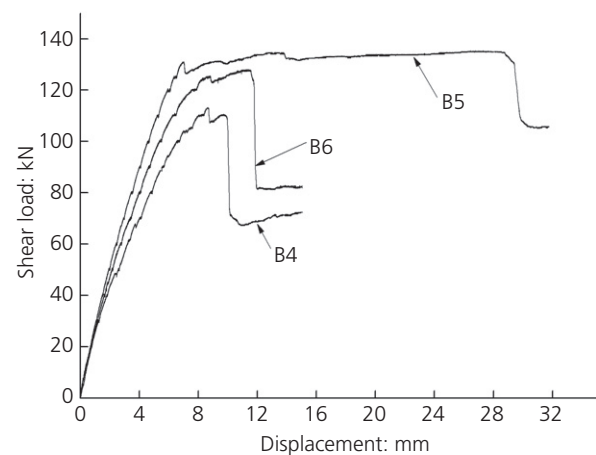


Figure 11. Shear load–displacement curves of B series of beams with stirrup ratio of 0.35%

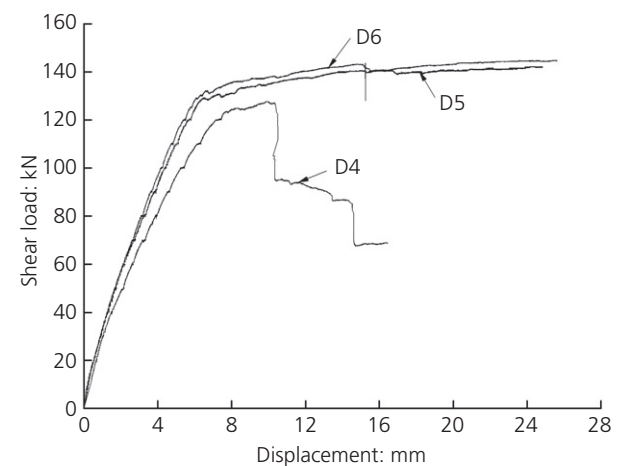
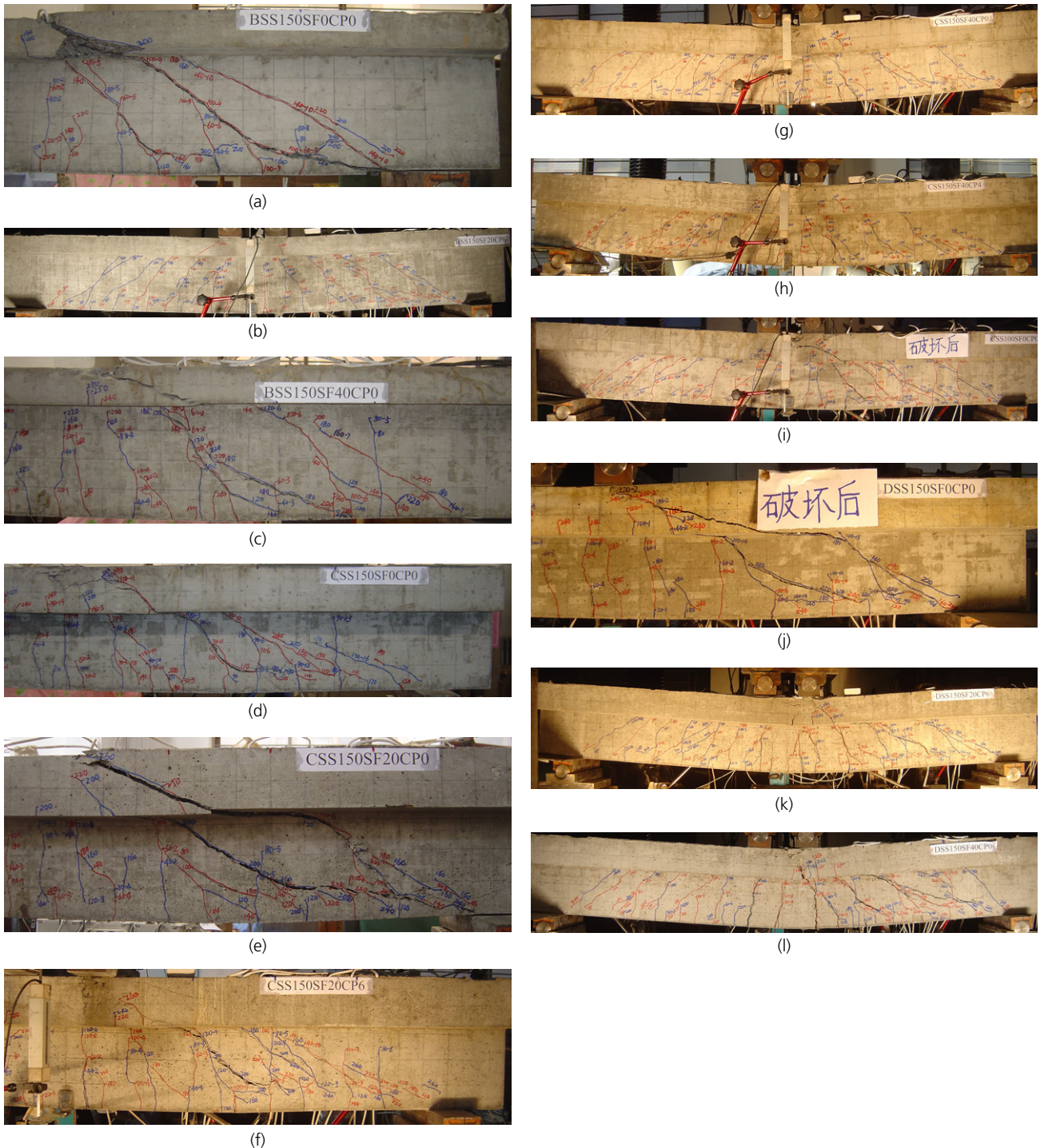


Figure 13. Shear load–displacement curves of D series of beams with stirrup ratio of 0.35%



**Figure 14.** Crack pattern and failure mode of B, C, D series of T-beams with stirrups: (a) B4; (b) B5; (c) B6; (d) C6; (e) C7; (f) C8; (g) C9; (h) C10; (i) C11; (j) D4; (k) D5; (l) D6

The influence of different flange sizes on the ultimate shear loads of B, C and D series of T-beams is shown in Figure 16. Observations from Figure 16 and Table 5 are given below.

With the exception of the C4 T-beam (steel fibre  $40 \text{ kg/m}^3$ , stirrup ratio 0%), the ultimate shear loads of C and D series of T-beams are better than those of the B series of T-beams. Apart from the T-beams without stirrups and fibres, the

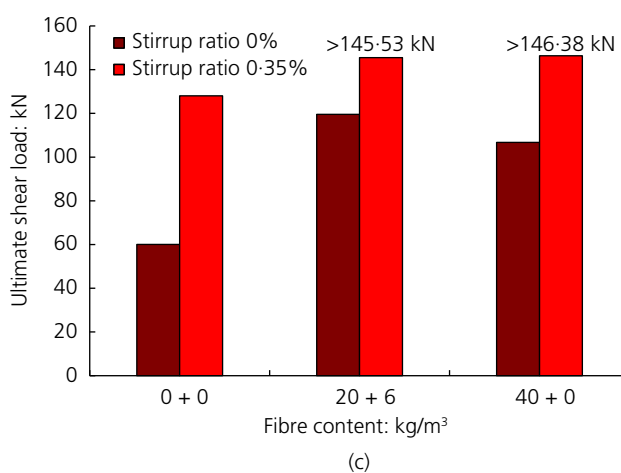
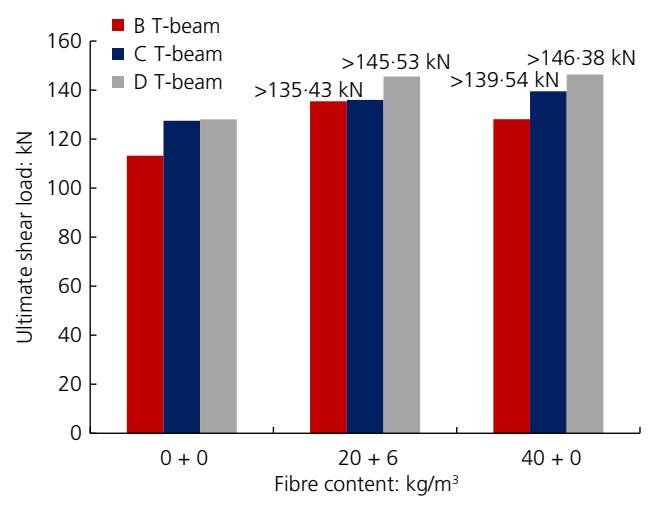
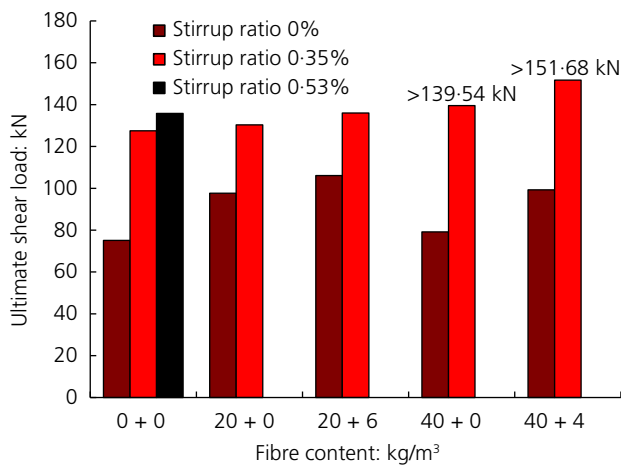
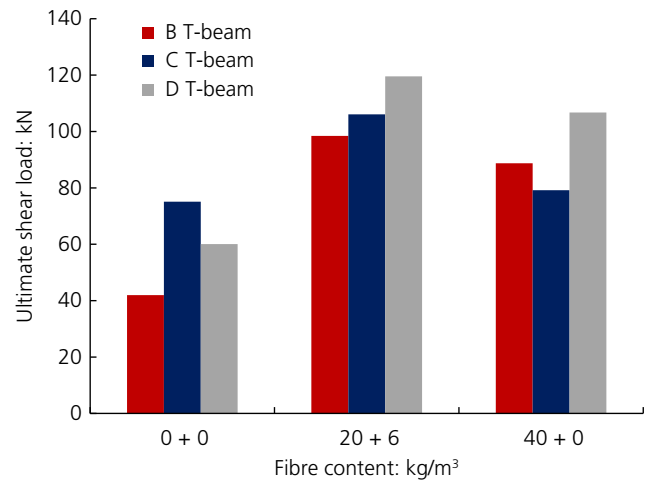
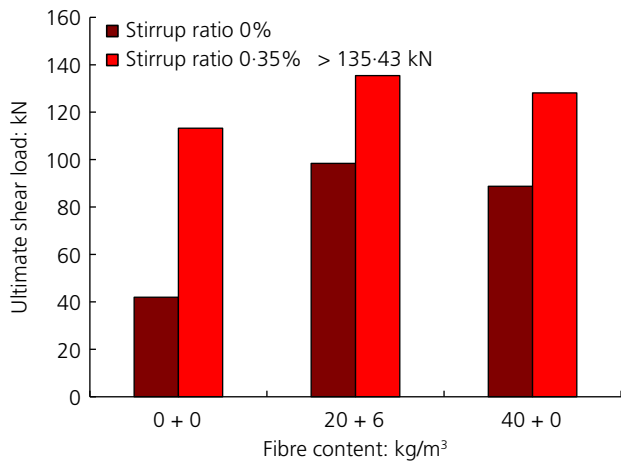


Figure 15. Influence of fibre contents on ultimate shear load of B, C, D series of T-beams: (a) B series of T-beams; (b) C series of T-beams; (c) D series of T-beams

Figure 16. Influence of different flange size on ultimate shear load: (a) stirrup ratio of 0%; (b) stirrup ratio of 0.35%

ultimate shear loads of the D series of T-beams are better than those of the C series of T-beams. This indicates that the ultimate shear load increased with the increase of flange size.

Therefore, when calculating the ultimate shear load of T-beams, different flange sizes should be considered.

#### Proposed predictive equations

There is no related formula in the references and codes to predict the ultimate shear load of hybrid-fibre-reinforced SCC T-beams. Based on related research by the present authors and other researchers in previous studies, three methods are proposed in this paper: the effective width, form factor and shear-funnel methods for predicting the ultimate shear load of steel fibre-reinforced SCC T-beams. Two other methods: the revised  $\sigma-w$  design method and the revised  $\sigma-\epsilon$  design method can predict the ultimate shear load of hybrid-fibre- or steel-fibre-reinforced SCC T-beams. These methods will be described in detail in the following subsections.

### Effective width

The shear strength of rectangular beams  $v_u$  at failure is defined as the ultimate shear load divided by beam width  $b$  and effective depth  $d$  ( $v_u = V/bd$ ). The average shear strength of rectangular beams with steel fibres and stirrups can be calculated according to Equation 1, as proposed in the literature (Ding *et al.*, 2011).

$$1. \quad v_{uf} = v_{uc} + v_s + v_f$$

where  $v_{uc}$  is the contribution of the concrete to shear strength;  $v_s$  is the contribution of the stirrups to shear strength; and  $v_f$  is the contribution of the fibres to shear strength.

$$2. \quad v_{uc} = v_a + v_b \\ = \zeta \left[ 0.97 \rho_s^{0.46} f_c^{1/2} + 0.2 \rho_s^{0.91} f_c^{0.38} f_{yl}^{0.96} (a/d)^{-2.33} \right]$$

with

$$\zeta = 1 / \sqrt{1 + d / (25d_a)}$$

$$\rho_s = A_s / (bd)$$

where  $v_a$  and  $v_b$  denote the shear stresses due to the arch and beam actions, respectively;  $\zeta$  denotes the factor for taking into account the size effect;  $d$  denotes the effective depth of the beam;  $d_a$  denotes the maximum size of coarse aggregate;  $f_c$  denotes the compressive strength of a circular cylinder;  $\rho_s$  denotes the longitudinal reinforcement ratio;  $f_{yl}$  denotes the yield strength of the longitudinal reinforcement; and  $a/d$  denotes the shear span–depth ratio.

$$3. \quad v_s = 1.75 I_b \rho_{st} f_{yst}$$

$$4. \quad I_b = \frac{0.97 \rho_s^{0.46} f_c^{1/2}}{0.97 \rho_s^{0.46} f_c^{1/2} + 0.2 \rho_s^{0.91} f_c^{0.38} f_{yl}^{0.96} (a/d)^{-2.33}}$$

$$\rho_{st} = A_{st} / (bs)$$

where  $I_b$  denotes the index of beam action;  $f_{yst}$  denotes the yield strength of the stirrup; and  $\rho_{st}$  denotes the stirrup ratio evaluated with reference to the spacing,  $s$ .

$$v_f = 0.5 \tau V_f \frac{l_f}{d_f} \cot \alpha$$

where  $\alpha$  denotes the inclination between the longitudinal reinforcement and the shear crack, and  $\alpha$  is assumed to be equal to 45°.

The ultimate shear load can be calculated by Equation 5.

$$5. \quad V_{uf} = V_{uc} + V_s + V_f$$

with

$$6. \quad V_{uc} = v_{uc} b d \\ = \zeta \left[ 0.97 \rho_s^{0.46} f_c^{1/2} + 0.2 \rho_s^{0.91} f_c^{0.38} f_{yl}^{0.96} (a/d)^{-2.33} \right] \\ \times b d$$

$$7. \quad V_s = v_s b d = 1.75 I_b \rho_{st} f_{yst} b d$$

$$8. \quad V_f = v_f b d = 0.5 \tau \rho_f l_f / d_f \cot \alpha b d$$

Based on the work of Zararis *et al.* (2006), the Equation 5 is revised using ‘effective width,  $b_{ef}$ ’ for calculating the ultimate shear load of the B, C and D series of T-beams.

Defining the effective width of a T-beam in shear,  $b_{ef} = A/c$ , where  $A$  equals the area of the shaded part of the cross-section and  $c$  equals the distance from the extreme compression fibre to the neutral axis (depth of compression zone), the following expression is derived

$$9. \quad b_{ef} = b_w \left[ 1 + 0.5 \times \frac{h_f}{d} \left( \frac{b_f}{b_w} - 1 \right) / \frac{c}{d} \right]$$

where  $h_f$  is the flange thickness;  $d$  is the effective depth;  $b_f$  is the flange width; and  $b_w$  is the web width, namely, the rectangular beam width,  $b$ .

The depth of the compression zone,  $c$ , is determined analytically after taking into account the shape of the compression zone, and is given by the positive root of the following equation (for further details, refer to the appendix in Zararis *et al.* (2006)) (see Figure 17).

$$\left( \frac{c}{d} \right)^2 + \left[ 1.5 \frac{h_f}{d} \left( \frac{b_f}{b_w} - 1 \right) + 600 \frac{\rho + \rho'}{f_c'} \right] \\ \times \frac{c}{d} - 600 \frac{\rho + (d'/d)\rho'}{f_c'} = 0$$

The effective width  $b_{ef}$  can replace the width  $b$  in Equation 6 for the ultimate shear load of a beam without stirrups. Therefore, Equation 10 for calculating the ultimate shear load of T-beams is derived and proposed

Based on the work of Tureyen *et al.* (2006), two other methods that consider the contribution of the flange to ultimate shear load can be used. These two methods are

$$10. \quad V_{uf} = V_{uc} + V_s + V_f = \xi \left[ 0.97 \rho_s^{0.46} f_c^{1/2} + 0.2 \rho_s^{0.91} f_c^{0.38} f_{yl}^{0.96} (a/d)^{-2.33} \right] \times b_{ef} d + 1.75 I_b \rho_w f_{yv} b d + 0.5 \tau \rho_f l_f / d_f \cot \alpha b d$$

the form factor and shear-funnel methods, and they are described below.

### Form factor

To evaluate the influence of the flange, it is suggested that the shear strength of T-beams based on the factor  $\sqrt{b_w/b_f}$  can be calculated according to Equation 11. It should be noted that the multiplier was developed for cases where the neutral axis is located within the flange thickness after cracking. Therefore, the multiplier should not modify the area of concrete in compression that is below the flange for members where the neutral axis depth calculated using elastic, cracked-section analysis is below the flange.

$$11. \quad \begin{aligned} v_c &= 5\sqrt{f'_c} \left( b_f c \sqrt{b_w/b_f} \right) && \text{when } c \leq t \\ v_c &= 5\sqrt{f'_c} \left[ b_f t \sqrt{b_w/b_f} + b_w(c-t) \right] && \text{when } c > t \end{aligned}$$

where  $c$  is the neutral axis depth calculated using an elastic cracked section analysis;  $t$  is the flange thickness;  $f'_c$  is the cylinder compressive strength;  $b_f$  is the flange width; and  $b_w$  is the web width. Because the term  $\sqrt{b_w/b_f}$  yields a value of 1 when there are no flanges, the form factor approach unifies the calculation of the shear strength of both T-beams and rectangular beams.

Considering the contribution of stirrups and fibres to the shear strength, Equations 3 and 4 were added to Equation 11. Equation 12, used to calculate the shear strength of T-beams, is thereby derived and proposed

$$12. \quad \begin{aligned} v_{uf} &= 5\sqrt{f'_c} \left( b_f c \sqrt{b_w/b_f} \right) + 1.75 I_b \rho_w f_{yv} + 0.5 \tau \rho_f l_f / d_f \cot \alpha && \text{when } c \leq t \\ v_{uf} &= 5\sqrt{f'_c} \left[ b_f t \sqrt{b_w/b_f} + b_w(c-t) \right] + 1.75 I_b \rho_w f_{yv} + 0.5 \tau \rho_f l_f / d_f \cot \alpha && \text{when } c > t \end{aligned}$$

Then, Equation 13, used to calculate the ultimate shear load of T-beams, is derived

$$13. \quad \begin{aligned} V_{uf} &= \left[ 5\sqrt{f'_c} \left( b_f c \sqrt{b_w/b_f} \right) + 1.75 I_b \rho_w f_{yv} + 0.5 \tau \rho_f l_f / d_f \cot \alpha \right] b d && \text{when } c \leq t \\ V_{uf} &= \left\{ 5\sqrt{f'_c} \left[ b_f t \sqrt{b_w/b_f} + b_w(c-t) \right] + 1.75 I_b \rho_w f_{yv} + 0.5 \tau \rho_f l_f / d_f \cot \alpha \right\} b d && \text{when } c > t \end{aligned}$$

### Shear funnel

Equation 11 considers the effect of the web-to-flange width ratio in determining the effective shear area in the flanges. Keeping all other variables constant, it is expected that the shear strength of a T-beam should increase as the flange thickness increases. This trend, however, is not accounted for using the form factor approach. While it is not expected that the flange thickness has a significant effect on the calculation of

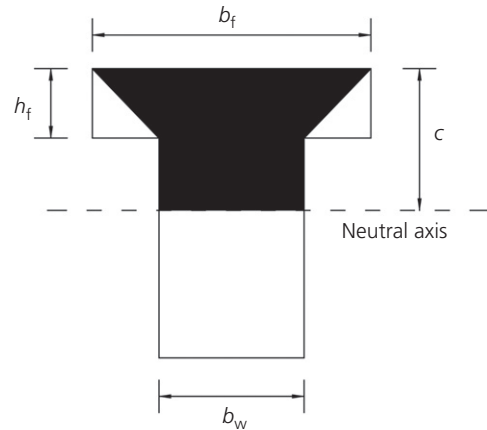


Figure 17. Cross-section of T-beam with effective shear area of concrete (shaded)

effective shear area for most practical T-beam geometries used in reinforced concrete construction, unusually thin or thick flanges may result in actual effective shear areas different from those calculated using the form factor approach.

To account for the effect of flange thickness on the effective shear area of a T-beam, the concept of a shear funnel was developed. This concept is illustrated in Figure 18. Two angled lines are extended from both corners of the web-to-flange interface into the flanges of a T-beam until they cross the top surface of the flange. Two cases, one with the neutral axis located in the flange and the other with the neutral axis in the

web, are illustrated in Figures 18(a) and 18(b). A third case where the lines intersect with the side faces of a T-beam flange may also occur when the flange width extending beyond the web is smaller than its thickness. In such cases, the effective shear area is also bounded by the side surfaces of the flange, as illustrated in Figure 18(c). According to the shear-funnel concept, the area of concrete bounded by the neutral axis and the two angled lines is defined as the effective shear area.

The largest angle  $\theta$  calculated was approximately  $42^\circ$ . Based on the analysis in the literature (Tureyen *et al.*, 2006), a value of  $45^\circ$  was selected as a simple and conservative value. The shear strength of T-beams without stirrups and fibres based on the concept of a shear funnel can be calculated according to Equation 14.

$$14. \quad \begin{aligned} v_c &= 5\sqrt{f'_c}b_wc[1 + (\text{Area} - b_wc)/b_wc] \\ &= 5\sqrt{f'_c}b_wc \times \text{Area}/b_wc \\ &= 5\sqrt{f'_c} \times \text{Area} \end{aligned}$$

where 'Area' refers to the effective shear area, see Figure 18.

Considering the contribution of stirrups and fibres to the shear strength, the Equations 3 and 4 were added to Equation 14. Equation 15, used to calculate the shear strength of T-beams, is thereby derived and proposed

$$15. \quad v_c = 5\sqrt{f'_c} \times \text{Area} + 1.75I_b\rho_vf_{yv} + 0.5\tau\rho_f l_f/d_f \cot \alpha$$

Then Equation 16, used to calculate the ultimate shear load of T-beams, is derived

$$16. \quad v_c = (5\sqrt{f'_c} \times \text{Area} + 1.75I_b\rho_vf_{yv} + 0.5\tau\rho_f l_f/d_f \cot \alpha)bd$$

#### Revised Rilem TC 162-TDF $\sigma$ - $\varepsilon$ design method

The ultimate shear load of a beam with shear reinforcement and containing steel fibres according to the Rilem TC 162-TDF  $\sigma$ - $\varepsilon$  design method is given by

$$17. \quad V_{Rd,3} = V_{cd} + V_{fd} + V_{wd}$$

where  $V_{cd}$  is the ultimate shear load of the member without shear reinforcement, given by

$$18. \quad V_{cd} = [0.12k(100\rho_s f_{ck})^{1/3} + 0.15\sigma_{cp}]b_w d \quad (N)$$

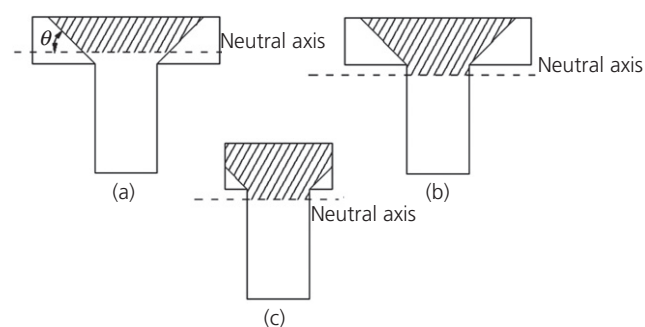


Figure 18. Shear funnel

$V_{fd}$  is the contribution of the steel fibre shear reinforcement, given by

$$19. \quad V_{fd} = 0.7k_f k_1 \tau_{fd} b_w d \quad (N)$$

and  $V_{wd}$  is the contribution of the shear reinforcement due to stirrups and/or inclined bars, given by

$$20. \quad V_{wd} = \frac{A_{sw}}{s} 0.9df_{ywd}(1 + \cot \alpha) \sin \alpha \quad (N)$$

The effective width  $b_{ef}$  in Equation 9 can replace the width  $b_w$  in Equation 18 for the ultimate shear load of beam without stirrups. Therefore, the Equation 21 used to calculate the ultimate shear load of T-beams is derived and proposed:

$$21. \quad \begin{aligned} V_{Rd,3} &= [0.12k(100\rho_s f_{ck})^{1/3} + 0.15\sigma_{cp}]b_{ef}d \\ &+ 0.7k_f k_1 \tau_{fd} b_w d + \frac{A_{sw}}{s} 0.9df_{ywd}(1 + \cot \alpha) \sin \alpha \end{aligned}$$

#### Revised Rilem TC 162-TDF $\sigma$ - $w$ design method

The ultimate shear load of a beam with shear reinforcement and containing steel fibres according to the Rilem TC 162-TDF  $\sigma$ - $w$  design method is also given by Equation 17. However, the difference of between the  $\sigma$ - $w$  design method and the  $\sigma$ - $\varepsilon$  design method lies in the calculation of the contribution of the steel fibre shear reinforcement. In the Rilem TC 162-TDF  $\sigma$ - $w$  design method, the fibre contribution  $V_{fd}$  is calculated from the design stress-crack opening relationship  $\sigma_{w,d}(w)$  in the following way

$$22. \quad V_{fd} = b_w z \bar{\sigma}_{p,d}(w_m)$$

with

$$23. \quad \bar{\sigma}_{p,d}(w_m) = \frac{1}{w_m} \int_0^{w_m} \sigma_{w,d}(u) du$$

where the quantity  $\bar{\sigma}_{p,d}(w_m)$  is called the mean design residual stress at the crack width  $w_m$  and represents the mean value of the post-cracking stress between zero and  $w_m$ .

The effective width  $b_{ef}$  in Equation 9 can also replace the width  $b_w$  in Equation 18 for the ultimate shear load of a beam without stirrups. Therefore, Equation 24, used to calculate the ultimate shear load of T-beams, is derived and proposed

$$24. \quad \begin{aligned} V_{Rd,3} &= [0.12k(100\rho_s f_{ck})^{1/3} + 0.15\sigma_{cp}]b_{ef}d \\ &+ b_w z \bar{\sigma}_{p,d}(w_m) + \frac{A_{sw}}{s} 0.9df_{ywd}(1 + \cot \alpha) \sin \alpha \end{aligned}$$

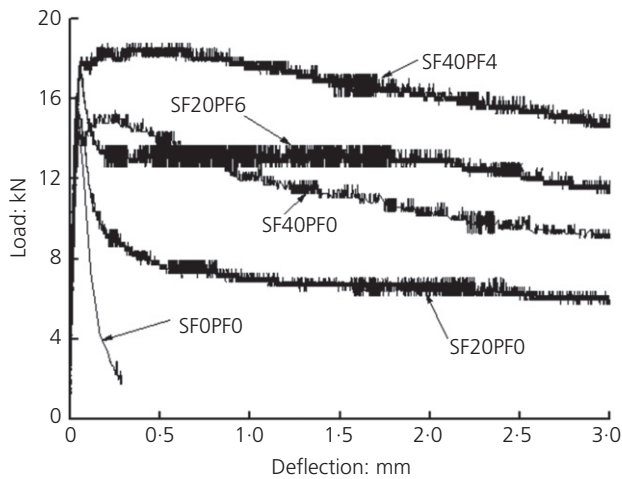


Figure 19. Load-deflection curves of hybrid-fibre-reinforced SCC

When the Rilem TC 162-TDF  $\sigma-\varepsilon$  design method and the Rilem TC 162-TDF  $\sigma-w$  design method have been used to calculate the ultimate shear load of T-beams, the load-deflection curves of hybrid-fibre-reinforced SCC should be tested. The load-deflection curves of hybrid-fibre-reinforced SCC using the notched beam test in the present study can be seen in Figure 19. The flexural strength and toughness of the hybrid-fibre-reinforced SCC are shown in Table 6.

The tensile stress-crack opening relationship of hybrid-fibre-reinforced SCC is determined by inverse analysis using the load plotted against crack mouth opening displacement curve from notched beam testing according to the Rilem TC 162-TDF  $\sigma-w$  design method. Because the load-deflection curves of a notched beam are proportional to the load plotted against crack mouth opening displacement curve, the tensile stress-crack opening relationship of hybrid-fibre-reinforced SCC can be determined by inverse analysis using the load-deflection curves of a notched beam. In this study, the bilinear stress-crack opening relationship is used, which is illustrated in Figure 20.

The parameters  $\alpha_1$  and  $\alpha_2$  are the slopes of the first and second linear curves, respectively. The parameter  $b_2$  is the Y-intercept of the second linear curve. The material parameters  $\alpha_1$ ,  $\alpha_2$  and  $b_2$  determined by inverse analysis are listed in Table 7.

Table 6. Flexural strength and toughness of hybrid-fibre-reinforced SCC

Fibre type	$f_t$ : MPa	$D_c$ : N mm	$D_{f2}$ : N mm	$D_{f3}$ : N mm	$f_{eq,2}$ : MPa	$f_{eq,3}$ : MPa	$f_{R,1}$ : MPa	$f_{R,2}$ : MPa	$f_{R,3}$ : MPa	$f_{R,4}$ : MPa
SFOPFO	5.17	1.20	—	—	—	—	—	—	—	—
SF20PFO	5.16	0.86	6.41	21.98	4.10	2.81	3.00	2.82	2.69	2.56
SF20PF6	5.04	0.87	8.32	31.20	5.33	3.99	3.79	3.79	3.74	3.66
SF40PFO	5.46	1.01	8.83	34.21	5.65	4.38	3.95	4.10	4.10	4.01
SF40PF4	5.14	0.90	10.06	37.01	6.44	4.74	4.53	4.57	4.47	4.33

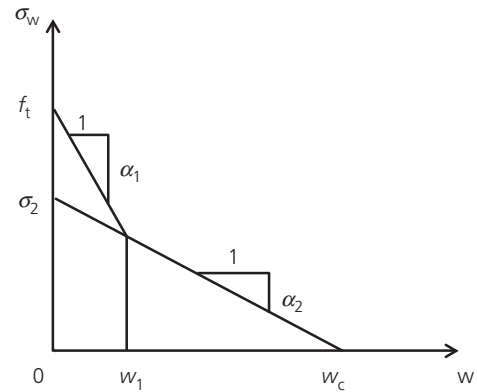


Figure 20. Bilinear stress-crack opening relationship

Table 7. Material parameters of beams based on inverse analysis

Fibre type	Material parameters		
	$\alpha_1$	$\alpha_2$	$b_2$
SF20PFO	18	0.05	0.29
SF20PF6	13	0.03	0.45
SF40PFO	63	0.19	0.5
SF40PF4	18	0.09	0.59

Figure 21 shows a comparison of the load-deflection curves between test and theory for beams SF20PF6 and SF40PF4. It can be seen that theoretical and experimental curves fit well based on the material parameters in Table 7.

The ultimate shear loads of T-beams containing hybrid fibres and/or with stirrups according to the revised Rilem TC 162-TDF  $\sigma-\varepsilon$  design method and the revised Rilem TC 162-TDF  $\sigma-w$  design method are calculated and listed in Table 8.

When the T-beams failed in flexure collapse, the shear load of the shear span of the T-beam did not reach the maximum. Therefore, the ultimate shear load of T-beams that failed in flexure collapse was not studied. Table 8 also gives the predicted value of ultimate shear load of T-beams with steel fibres using the effective width, form factor and shear-funnel methods. The ratios of experimental ultimate shear load to the predicted values ( $V_{test}/V_{predicted}$ ) are listed in Table 8 as well.

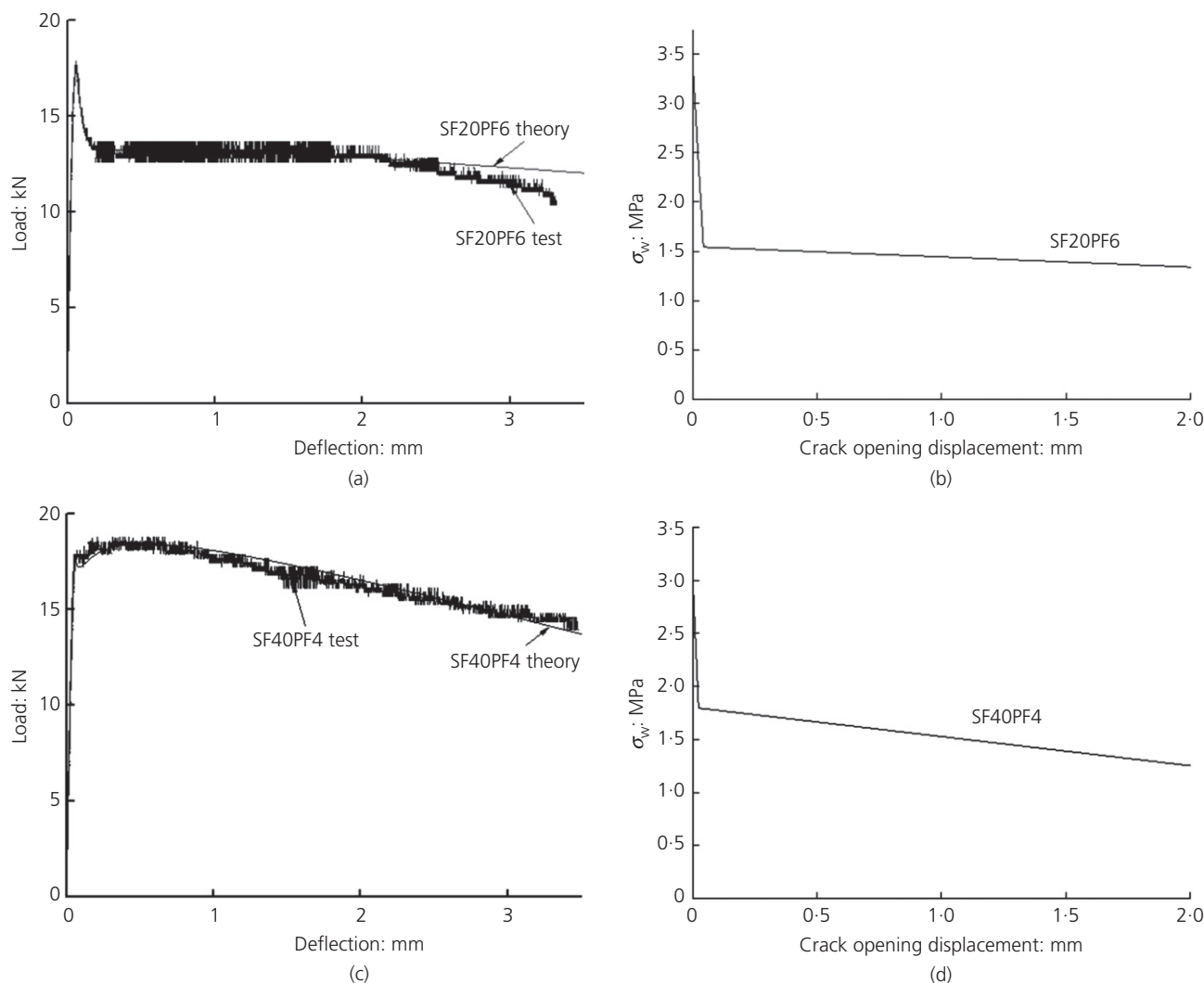


**Figure 21.** Comparison of load–deflection curves between test and theory of beams SF20PF6, SF40PF4: (a) comparison of load–deflection curves between test and theory for beam SF20PF6; (b) tensile stress–crack opening relationship for beam SF20PF6; (c) comparison of load–deflection curves between test and theory for beam SF40PF4; (d) tensile stress–crack opening relationship for beam SF40PF4

The average and coefficient of variation of hybrid-fibre-reinforced SCC T-beams are calculated and listed in Table 8.

Research studies investigating the influence of hybrid fibres on the shear behaviour of T-beams are few. Methods described as the revised  $\sigma-w$  design method and revised  $\sigma-\epsilon$  design method should be used based on the load–deflection curves of fibre-reinforced SCC using the notched beam test. The load–deflection curves from the notched beam test are not usually given in the literature. Therefore, the proposed methods for predicting ultimate shear load of fibre-reinforced T-beams only were used for T-beams in this text. Although the sample was small, some meaningful results can be obtained from this study. From Table 8, the following points can be observed.

- The ultimate shear load of T-beams containing hybrid fibres and/or with stirrups (or steel fibres) can be predicted by the revised  $\sigma-w$  design method and the revised  $\sigma-\epsilon$  design method. The effective width, form factor and shear-funnel methods can only predict the ultimate shear load of T-beams with stirrups and/or containing steel fibres.
- No matter whether the T-beam is without stirrups or contains stirrups, the predicted values of ultimate shear load of the T-beam are very conservative using the form factor and shear-funnel methods.
- For a T-beam without stirrups, the values predicted by the effective width method are overestimated. The mean ratio  $V_{\text{test}}/V_{\text{predicted}}$  for a steel-fibre-reinforced SCC T-beam without stirrups is 0.9.

Table 8. Ultimate shear load, average and coefficient of variation of T-beams

Fibre type	Test data: kN	Predicted value: kN					Test data/Predicted value				
		Revised $\sigma-w$ design method	Revised $\sigma-\epsilon$ design method	Effective width	Form factor	Shear funnel	Revised $\sigma-w$ design method	Revised $\sigma-\epsilon$ design method	Effective width	Form factor	Shear funnel
B1	41.95	45.6	45.60	61.63	43.03	45.42	0.92	0.92	0.68	0.97	0.92
B2	98.44	85.1	66.31	—	—	—	1.16	1.48	—	—	—
B3	88.75	75.9	63.18	79.42	64.55	66.40	1.17	1.40	1.12	1.37	1.34
C1	75.12	52.41	52.41	72.25	40.11	49.67	1.43	1.43	1.04	1.87	1.51
C2	97.63	72.84	67.65	85.53	53.66	62.95	1.34	1.44	1.14	1.82	1.55
C3	106.10	91.94	75.26	—	—	—	1.15	1.41	—	—	—
C4	79.15	82.03	71.59	86.86	62.16	70.13	0.96	1.11	0.91	1.27	1.13
C5	99.26	88.86	74.21	—	—	—	1.12	1.34	—	—	—
D1	60.05	81.40	81.40	118.20	32.94	39.58	0.74	0.74	0.51	1.82	1.52
D2	119.58	121.20	106.29	—	—	—	0.99	1.13	—	—	—
D3	106.75	108.07	99.56	118.47	55.78	61.63	0.99	1.07	0.90	1.91	1.73
				Average		Average	1.09	1.22	0.9	1.58	1.39
				Coefficient of variation		Coefficient of variation	0.17	0.19	0.24	0.22	0.19
B4	113.23	75.6	75.60	94.5	75.97	78.36	1.69	1.69	1.36	1.69	1.63
B6	128.11	105.9	93.18	112.36	97.48	99.34	1.07	1.22	1.01	1.16	1.14
C6	127.50	82.41	82.41	105.19	73.05	82.61	1.55	1.55	1.21	1.75	1.54
C7	130.29	102.84	97.65	118.47	86.59	95.89	1.27	1.33	1.10	1.50	1.36
C8	135.99	121.94	105.26	—	—	—	1.12	1.29	—	—	—
C11	135.80	97.42	95.24	121.66	89.52	99.08	1.39	1.43	1.12	1.52	1.37
D4	128.05	111.40	111.40	151.14	65.88	72.52	1.15	1.15	0.85	1.94	1.77
				Average		Average	1.32	1.38	1.11	1.59	1.47
				Coefficient of variation		Coefficient of variation	0.16	0.13	0.14	0.15	0.16

- (d) For a T-beam without stirrups, the mean ratio  $V_{test}/V_{predicted}$  using the revised  $\sigma-w$  design method is 1.09. The predicted ultimate shear load is safe and acceptable in relation to the experimental values. The coefficient of variability is 0.17. Thus the proposed Equation 24 using the revised  $\sigma-w$  design method shows good applicability. The revised  $\sigma-w$  design method is better than the revised  $\sigma-\epsilon$  design method for estimating the ultimate shear load of T-beams without stirrups. However, the revised  $\sigma-w$  design method is more complicated.
- (e) For SCC T-beams with stirrups, the values predicted by the effective width method are relatively close to the experimental values. The mean ratio  $V_{test}/V_{predicted}$  using the effective width method is 1.11. However, this method can only predict the ultimate shear load of steel-fibre-reinforced SCC T-beams.
- (f) For hybrid-fibre-reinforced SCC T-beams with stirrups, the values predicted by the revised  $\sigma-w$  design method are safe and relatively conservative. The revised  $\sigma-w$  design method is also better than the revised  $\sigma-\epsilon$  design method for estimating the ultimate shear load of T-beams with stirrups.

Therefore, the revised  $\sigma-w$  design method is more suitable for predicting the ultimate shear load for beams containing hybrid fibres and/or with stirrups than the other methods. However,

further experiments and research should be done in future to verify the applicability of the revised  $\sigma-w$  design method.

### Conclusions

The shear behaviour of three series of hybrid-fibre-reinforced SCC T-beams was studied. The influence of the fibre, the composite effects of the steel bars and fibre, and the influence of the flange size on the ultimate shear load of SCC T-beams were ascertained. Based on the analysis of the test results presented herein, the following conclusions can be drawn.

- (a) Results showed that the mechanical behaviour of the T-beam with hybrid fibres is much better than that of a T-beam without stirrups and fibres or only with mono-steel fibres.
- (b) The addition of hybrid fibres in adequate amounts can change the failure mode of a brittle shear failure into a ductile flexural mechanism. The B5 T-beam (with stirrup ratio of 0.35% and hybrid fibres 20 + 6 kg/m<sup>3</sup>), the C10 T-beam (with stirrup ratio of 0.35% and hybrid fibres 40 + 4 kg/m<sup>3</sup>) and the D5 T-beam (with stirrup ratio of 0.35% and hybrid fibres 20 + 6 kg/m<sup>3</sup>) all failed in flexural collapse.
- (c) Hybrid fibres can evidently enhance the ultimate shear load for each stirrup ratio. Compared to mono-steel fibres, the ultimate shear loads of T-beams with the

addition of hybrid fibres  $20 + 6 \text{ kg/m}^3$  are better than those of T-beams with steel fibres  $40 \text{ kg/m}^3$ .

- (d) The influence of different flange sizes on the ultimate shear load of T-beams should be considered. The ultimate shear load increased with the increase of flange size.
- (e) Three methods were proposed – the effective width, form factor and shear-funnel methods – for predicting the ultimate shear load of steel-fibre-reinforced SCC T-beams, and another two methods were proposed – the revised  $\sigma-w$  design method and the revised  $\sigma-\varepsilon$  design method – for predicting the ultimate shear load of hybrid-fibre- or steel-fibre-reinforced SCC T-beams. The ultimate shear loads recorded experimentally were compared with the values obtained from the proposed equations. The revised  $\sigma-w$  design method was found to be more suitable for predicting the ultimate shear load of T-beams containing hybrid fibres and/or with stirrups, and the correlation was satisfactory.

## Acknowledgements

The authors gratefully acknowledge the North China University of Science and Technology Foster Fund Project (GP201523), Hebei Province Natural Science Fund Project (E2012401044), State Key Laboratory of coastal and offshore engineering of Dalian University of Technology Fund Project (LP1209) and National Natural Science Foundation of China (NSFC) (grant nos 51478162 and 51478161).

## REFERENCES

- Abadel A, Abbas H, Almusallam T, Al-Salloum Y and Siddiqui N (2016) Mechanical properties of hybrid fibre-reinforced concrete – analytical modelling and experimental behaviour. *Magazine of Concrete Research* **68(16)**: 823–843, <http://dx.doi.org/10.1680/jmacr.15.00276>.
- ACI (American Concrete Institute) (2002) ACI 318-02: Building code requirements for structural concrete and commentary. American Concrete Institute, Farmington Hills, MI, USA.
- BSI (2004) BS EN 1992-1-1:2004: Design of concrete structures. General rules and rules for buildings. BSI, London, UK.
- Cucchiara C, Mendola LL and Papia M (2004) Effectiveness of stirrups and steel fibres as shear reinforcement. *Cement and Concrete Composites* **26(7)**: 777–786.
- Ding YN, Wang YH and Dong XJ (2005) An investigation on the workability of fiber reinforced self-compacting high performance concrete. *China Civil Engineering Journal* **38(11)**: 51–57 (in Chinese).
- Ding YN, Liu SG, Zhang YL and Thomas A (2008) The investigation on the workability of fibre cocktail reinforced self-compacting high performance concrete. *Construction and Building Materials* **22(7)**: 1462–1470.
- Ding YN, You ZG and Jalali S (2010) Hybrid fiber influence on strength and toughness of RC beams. *Composite Structures* **92(9)**: 2083–2089.
- Ding YN, You ZG and Jalali S (2011) Composite effect of hybrid fibers and stirrups on shear behavior of SCC beams. *Engineering Structures* **33(1)**: 107–117.
- Ding YN, Zhang FS, Torgal F and Zhang YL (2012) Shear behaviour of steel fibre reinforced self-consolidating concrete beams based on the modified compression field theory. *Composite Structures* **94(8)**: 2440–2449.
- Efnarc (European Federation of National Associations Representing Concrete) (2002) *EFNARC 2002: Specification and Guidelines for Self-Compacting Concrete*. Efnarc, Farnham, UK.
- EPG (The European Project Group) (2005) *SCC 028: The European Guidelines for Self-Compacting Concrete – Specification, Production and Use*. The SCC European Project Group, Farnham, UK.
- Ganesan N, Indira PV and Sabeena MV (2016) Constitutive behaviour of confined hybrid fibre reinforced HPC under uniaxial compression. *Magazine of Concrete Research* **68(1)**: 1–11, <http://dx.doi.org/10.1680/jmacr.14.00238>.
- Giaccio C, Mahaidi RA and Taplin G (2006) Flange strain measurement in shear critical RC T-beams. *Advances in Structural Engineering* **9(4)**: 491–505.
- Greenough T and Nehdi M (2008) Shear behavior of fiber-reinforced self-consolidating concrete slender beams. *ACI Materials Journal* **105(5)**: 468–477.
- Han SW, Lee CS, Kwon HW, Lee KH and Shin MS (2015) Behaviour of fibre-reinforced beams with diagonal reinforcement. *Magazine of Concrete Research* **67(24)**: 1287–1300, <http://dx.doi.org/10.1680/jmacr.14.00194>.
- Kwak YK, Eberhard MO, Kim WS and Kim J (2002) Shear strength of steel fibre-reinforced concrete beams without stirrups. *ACI Structural Journal* **99(4)**: 530–537.
- Ministry of Housing and Urban-Rural Construction of the People's Republic of China (2010) GB 50010-2010: Code for design of concrete structures. China Architecture & Building Press, Beijing, China (in Chinese).
- Tureyen AK, Wolf TS and Frosch RJ (2006) Shear strength of reinforced concrete T-beams without transverse reinforcement. *ACI Structural Journal* **103(5)**: 656–663.
- Zararis LP, Karaveziroglou MK and Zararis PD (2006) Shear strength of reinforced concrete T-beams. *ACI Structural Journal* **103(5)**: 693–670.
- Zhang FS, Ding YN and Xu J *et al.* (2016) Shear strength prediction for steel fiber reinforced concrete beams without stirrups. *Engineering Structures* **127(11)**: 101–106.

## How can you contribute?

To discuss this paper, please submit up to 500 words to the editor at [journals@ice.org.uk](mailto:journals@ice.org.uk). Your contribution will be forwarded to the author(s) for a reply and, if considered appropriate by the editorial board, it will be published as a discussion in a future issue of the journal.